Journal of Alloys and Compounds 554 (2013) 214–220

Contents lists available at SciVerse ScienceDirect

Journal of Alloys and Compounds

journal homepage: www.elsevier.com/locate/jalcom

Synthesis, spectral and surface investigation of $NaSrBO_3$: Sm^{3+} phosphor for full color down conversion in LEDs

Vinay Kumar [a,b,*], A.K. Bedyal [a], Shreyas S. Pitale [b], O.M. Ntwaeaborwa [b], H.C. Swart [b]

[a] School of Physics, Shri Mata Vaishno Devi University, Katra 182320 (J&K), India
[b] Department of Physics, University of the Free State, P.O. Box 339, Bloemfontein 9300, South Africa

ARTICLE INFO

Article history:
Received 29 August 2012
Received in revised form 20 November 2012
Accepted 21 November 2012
Available online 5 December 2012

Keywords:
Phosphors
XPS
ToF SIMS
Orthoborates
Luminescence

ABSTRACT

Orange–red emitting $NaSrBO_3$: Sm^{3+} phosphors were prepared by the combustion method using metal nitrates as precursors and urea as fuel. The particle sizes were in the range of 38–43 nm. The monoclinic structure that is in good agreement with the standard $NaSrBO_3$ was confirmed by X-ray diffraction. Scanning electron microscopy (SEM) indicated that an agglomerated peanut like morphology was obtained. UV–VIS spectrocsopy, photoluminescence (PL) and cathodoluminescence (CL) spectroscopy were utilized to investigate the spectral properties of the phosphor. The chemical states and the distribution of the dopants in the host were analysed with X-ray photoelectron spectroscopy (XPS) and time of flight-secondary ion mass spectroscopy (TOF-SIMS), respectively. Under the excitation of near UV light, $NaSrBO_3$: Sm^{3+} exhibits the characteristic emissions resulting for the $^4G_{5/2} \rightarrow {}^6H_{x/2}$ ($x = 5$, 7 and 9) transitions of Sm^{3+}, with a maximum intensity at 599 nm. In addition, the concentration of Sm^{3+} was varied in order to determine the optimum PL emission intensity. A maximum intensity was obtained from the sample with 2.0 mol% of Sm^{3+}. The potential applications of this phosphor, as a down conversion phosphor with an excitation wavelength of 395 nm and good CL intensity, are evaluated for the possible use as a high-color-purity phosphor in light emitting diodes (LEDs) that can fill the 590–600 nm gap and it may also be used as an amber color field emission display (FED) phosphor.

1. Introduction

In recent years, the alkali (A) – alkaline earth (E) ortho-borates with a general formula $AEBO_3$ have captured much attention of various researchers due to their potential application as new phosphor materials in solid state lighting. There are a variety of real and possible applications of such kind of materials used in light emitting diodes [1–4], FED applications [5], thermo-luminescence dosimetry [6,7], and also as controlled white light emitting phosphors [8–10]. White light emitting $Ca_xSr_{1-x}Al_2O_4$:Tb^{3+}/Eu^{3+} [11] and tuneable $Sr_xCa_{1-x}Al_2O_4$:Eu^{2+}/Dy^{3+} [12] phosphors were synthesized using different methods in the past. The white light generated was a combination of simultaneous blue and green narrow line emission from Tb^{3+} and the red emission from Eu^{3+} compared to the broadband emission from the Eu^{2+} and Dy^{3+}. The white light emission was only observed when excited at 227 nm. Wu et al. [13] initiated the research on orthoborate phosphor materials due to their interesting spectral and luminescent properties. Since then, the different hosts related to the alkali alkaline earth orthoborate family have been prepared and they are used in the development of phosphors for display technology. These orthoborates materials have many advantages such as low thermal conductivity, high melting point, high thermal expansion coefficient, high stability and ability to accommodate defects. $Lu_{0.8}Sc_{0.2}BO_3$:Eu^{3+}, Tb^{3+} can be used for an X-ray medical imaging system [14]. The stability and efficiency of the cathodoluminescence (CL) $LiSrBO_3$:Sm^{3+} phosphor [5] make it more suitable for applications in field emission displays (FEDs) where the prime operating conditions are the low electron beam accelerating voltage. Sm^{3+} doped phosphors have attracted much attention because of their peculiar orange–red emission. Mueller-Mach et al. [15] pointed out that there is an efficiency gap around 560 nm, which has been called the "yellow gap" [16], which fairly seriously extends into the amber range of 590–600 nm in the ranges of wavelengths covered by reasonably efficient diodes made from either III-nitrides or III-phosphides. Traditionally amber LEDs have been used in automotive applications for turn and day-time-running lights of cars and in traffic signals. Although the down conversion of blue light from InGaN LEDs by suitable color converters, especially phosphors, has become a dominant technique for producing white light for all kinds of applications, the down conversion of blue LED emission to produce 'monochromatic' or high-color-purity light, however, has been discussed only rarely [17,18]. The invention of the blue light emitting

* Corresponding author at: School of Physics, Shri Mata Vaishno Devi University, Katra 182320 (J&K), India. Tel.: +91 1991 285699x2509; fax: +91 1991 285694.
E-mail addresses: vinaykdhiman@yahoo.com, vinaykumar@smvdu.ac.in (V. Kumar).

0925-8388/$ - see front matter © 2012 Elsevier B.V. All rights reserved.
http://dx.doi.org/10.1016/j.jallcom.2012.11.125

diode based on GaN [19] and the use of the MOCVD technique for LED chip production have changed the trajectory of this field. It is possible to vary the emission wavelength of GaN-based blue LED's between 370 nm (band-gap of pure GaN), and 470 nm by increasing the In content in InGaN devices. The excitation spectrum obtained from Sm^{3+}-doped $LiSr_{0.8}Ba_{0.2}PO_4$ monitored at 595 nm consists of several bands centered at 360 nm, 373 nm, 401 nm and 467 nm, respectively, which are the characteristic f–f transitions of Sm^{3+} ions [20]. The strongest peak at 401 nm is attributed to the $^6H_{5/2} \rightarrow {}^4G_{7/2}$ transition of Sm^{3+}, making Sm^{3+} an excellent dopant candidate for excitation at around 400 nm and emission at around 595 nm. Furthermore with the development of nanotechnology, the optical properties of nanosized phosphors have been extensively investigated for their potential application in high resolution images and for fundamental research. It is therefore worthwhile to develop the nanosized phosphors to explore their properties and possible application in lighting.

Different method including the high temperature solid-state and combustion have been used for orthoborate synthesis. In this study, mixed orthoborate phosphors were prepared by using the combustion method with metal nitrates as precursors and urea as fuel. The versatility of the orthoborates and the unique excitation and emission of Sm^{3+} make it an excellent candidate for the "yellowgap" phosphor. Recently, combustion synthesis has been used to synthesis the $NaSrBO_3:Tb^{3+}$ phosphors by Nagpure et al. [21]. They have focused on the thermoluminescent properties of these phosphors. We evaluated the spectral and structural properties of the $NaSrBO_3:Sm^{3+}$ phosphors for a possible application in light emitting devices of different types. Special attention was given to determine if the synthesized the $NaSrBO_3:Sm^{3+}$ phosphor meet with the requirements that the excitation wavelength is in the 370–470 nm range (for InGaN–LED chip) and the emission in the 590–600 nm range (amber range).

2. Experimental details

High-purity sodium nitrate [$NaNO_3$], strontium nitrate [$Sr(NO_3)_2$], boric acid [H_3BO_3], samarium(III) nitrate pentahydrate [$Sm(NO_3)_3.5H_2O$], and urea (H_2NCONH_2) from Merck Chemicals were used as starting materials. $NaSrBO_3:Sm^{3+}$ (0.1–3.0 mol.%) was prepared by heating rapidly an aqueous solution containing weighed amounts of metal nitrates and urea in a pre-heated furnace maintained at 550 °C. Urea was used as a fuel for combustion, and its amount was calculated using total oxidizing and reducing valences. The aqueous solution underwent rapid dehydration and foaming followed by decomposition, generating combustible gases. These volatile combustible gases ignited and burned with a flame, yielding a voluminous solid. The whole combustion process was completed within 5 min. After the combustion process, the ashes were cooled to room temperature and crushed to a fine powder. For complete crystallinity, all samples were annealed for 2 h at 800 °C in air.

The particle morphology of these phosphors was analyzed by using a Shimadzu SSX-550 SuperScan scanning electron microscopy (SEM). A Bruker D8 Advance diffractometer was used to examine the purity and the phase homogeneity of the phosphors. The photoluminescence excitation and emission (in phosphorescence mode) spectra were measured at room temperature by using a VARAIN Cary-Eclipse spectrofluorometer equipped with a Xenon lamp that was used as an excitation source. Cathodoluminescence (CL) measurements were carried out in a vacuum chamber from PREVAC equipped with an ES40C electron gun power supply unit and USB2000+ spectrometer under different accelerating voltages and emission currents in a base pressure of $\sim 2 \times 10^{-8}$ torr. The XPS measurements were conducted using a PHI 5000 versa probe spectrometer using monochromatic Al Kα radiation ($h\nu$=1253.6 eV). For higher resolution spectra, the hemispherical analyzer pass energy was maintained at 11.3 eV. Measurements were performed using a 1 eV/step (or 45 min acquisition times) binding energies for survey scans from 0 to 1400 eV and 1 eV/step and 20–30 min times for the high resolution scans. A low energy electron beam was used to achieve charge neutrality at the sample surface. All the absolute binding energies of the photoelectron spectra were referenced to the monitored C 1s signal at 284.6 eV.

The dopant distribution analysis in the host lattice was carried out by using a TOF-SIMS IV (Ion-TOF, Munster, Germany) reflectron-type time-of-flight (ToF) mass spectrometer equipped with a bismuth ion gun. Pulsed 25 keV Bi^+ was used as primary ions with an ion current of 1.0 pA. SIMS spectra were measured by scanning over the 200 μm × 200 μm analysis area.

3. Results and discussion

3.1. Structural studies

The XRD patterns of the $NaSrBO_3:Sm^{3+}$ (2 mol.%), before and after annealing as well as the $NaSrBO_3$ standard are shown in Fig. 1. The peaks match well with the standard file peaks, which indicated that the doped Sm^{3+} ions have no obvious influence on the structure of the host, which suggests that the dopants were uniformly distributed inside the host matrix. In addition, the diffraction peak positions and the relative intensities of the samples are well matched with those reported in the literature [22], which belong to the monoclinic structure of P21/c. The average crystallite sizes were estimated by the well known Debye–Scherrer formula [23] from the line width of the main reflection and were found to be in the range between 38 and 43 nm. It must be pointed out that extra peaks at 30°, 32°, and 42.5° were obtained, which indicates that some impurity phases were present in the synthesized material.

The particle morphology of the as prepared and annealed sample was examined by SEM. To prevent charging, all samples were coated with an ultrathin layer of gold (Au). Fig. 2 shows the expected fluffy morphology of the particles normally obtained from the combustion synthesis. The voids are due to the large gaseous matter that escaped due to high exothermicity.

After annealing, the peanut-like agglomerated morphology was observed, which may be attributed to the melting nature of this system. The magnified images at different scales are also shown in Fig. 2 in this further confirms an agglomeration of peanut like particle morphology. Fig. 3 shows the diffuse reflectance spectrum of the $NaSrBO_3:Sm^{3+}$ (2 mol.%). The strong absorption band at 200–250 nm can be assigned to the $O^{2-} \rightarrow Sm^{3+}$ charge transfer bond (CTB) and the multiple spectral features from 345 nm to 474 nm can be assigned to the 4f–4f shell transitions of the Sm^{3+}, respectively [24]. Fig. 4 shows the photoluminescence (PL) excitation and emission spectra of the $NaSrBO_3:Sm^{3+}$ (2 mol.%). The excitation spectra were recorded in the 200–410 nm wavelength range and the emission peak has a maximum at 599 nm.

The excitation spectra consists of less intense 4f–4f transitions of Sm^{3+} at 346 nm, 365 nm, 376 nm and 395 nm and a strong band at 220–250 nm which is consistent with the strong absorption band assigned to a charge transfer process observed in the diffuse reflectance measurement. In the PL emission spectrum (recorded at 395 nm excitation), the peaks at 564 nm, 599 nm (prominent one) and 645 nm can be assigned, respectively, to the $^4G_{5/2} \rightarrow {}^6H_{5/2}$, $^4G_{5/2} \rightarrow {}^6H_{7/2}$ and $^4G_{5/2} \rightarrow {}^6H_{9/2}$ transition of the Sm^{3+} ion. It is clear that this phosphor could efficiently be excited by near-ultraviolet light-emitting diodes (380–400 nm) and it is be-

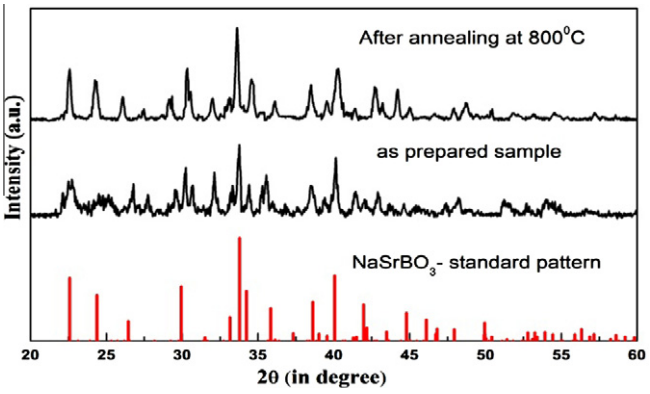

Fig. 1. XRD pattern of $NaSrBO_3:Sm^{3+}$ phosphors.

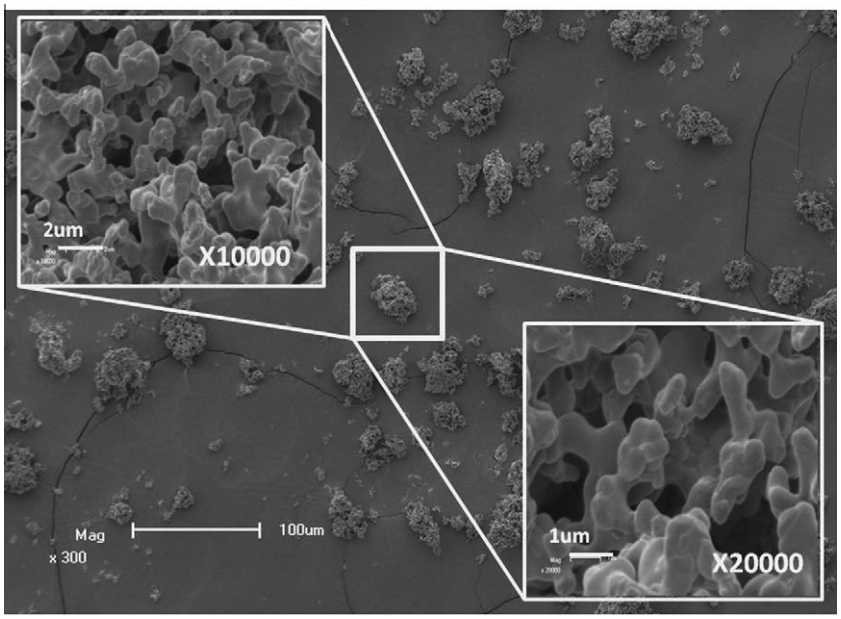

Fig. 2. SEM images of annealed $NaSrBO_3:Sm^{3+}$ phosphor at different magnification.

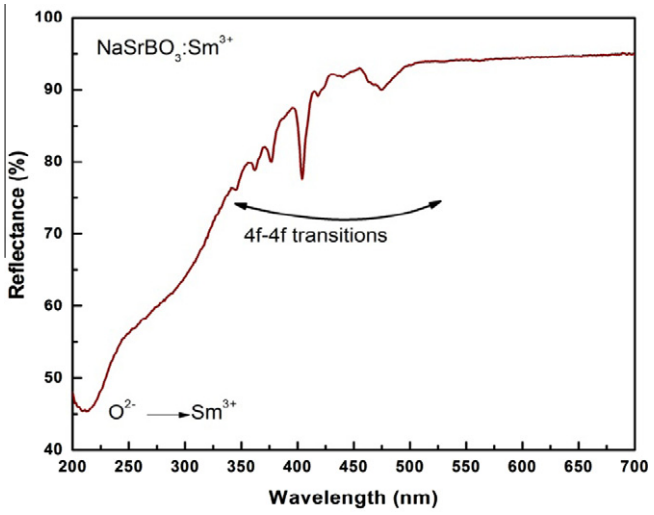

Fig. 3. Diffuse reflectance spectra of the $NaSrBO_3:Sm^{3+}$ phosphor.

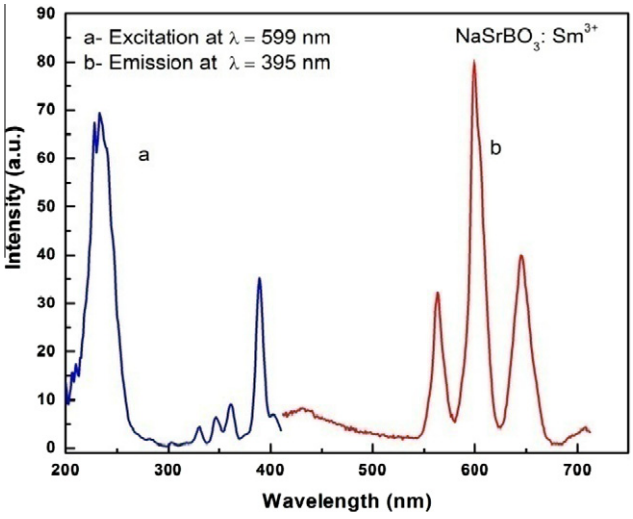

Fig. 4. Photoluminescence (a) excitation and (b) emission spectra of the $NaSrBO_3:Sm^{3+}$ phosphors.

lieved to be a promising orange–red (amber) emitting lamp phosphor for the "yellow gap" light-emitting diodes as explained in the introduction. Currently, efficient emitters have been demonstrated in the 400 nm regime. In fact, the highest-reported efficiency in an InGaN-based emitter has the power conversion efficiency of 21% for a ~400 nm LED, which is similar to this $NaSrBO_3:Sm^{3+}$ phosphor that is excited by 395 nm.

The blue LED plus phosphor strategy has the shortest time line for commercialization. Some companies already have demonstrated "white-light" generation by using a blue LED and a single phosphor to create white light. In some cases as in this case the UV/blue light emitted by the LED is converted by the phosphor to an amber color. The down conversion of the UV/blue light to amber colored light is complimentary to the blue light emitted by the LED.

The CL spectra of the $NaSrBO_3:Sm^{3+}$ (2 mol.%) nanophosphor that were recorded at different beam voltages of 2 keV, 3 keV and 4 keV, respectively, keeping the emission current constant at 800 μA (*please note*: *it is not the beam current*) are shown in Fig. 5. The peaks are similar to those observed in the PL emission spectrum in Fig. 4, except that the prominent emission was in the red spectral region at 602 nm corresponding to the $^4G_{5/2} \rightarrow {}^6H_{7/2}$ transition of the Sm^{3+} ion. The CL intensity increased with an increase accelerating voltage [25] from 2 keV to 4 keV due to an increase in penetration depth of the electron, creating a larger excitation volume.

Considerable changes in the luminescence intensity were observed (Fig. 6) as the Sm^{3+} ion concentration was varied. Increasing the Sm^{3+} ion concentration from 0.5 mol.% to 2.0 mol.% increased the luminescence intensity, whereas increasing the concentration of Sm^{3+} beyond 2.0 mol.% decreased the intensity. This may be ascribed to well known concentration quenching effects in luminescence phenomena [26]. The CIE 1931 chromaticity diagram for the $NaSrBO_3:Sm^{3+}$ nanocrystalline phosphor under 395 nm excitation is displayed in Fig. 7. It can be seen from the Fig. 7 that the CIE coordinates (x, y) of (0.5406, 0.3928) correspond to the shade of orange–red Sm^{3+} (2.0 mol.%) emission.

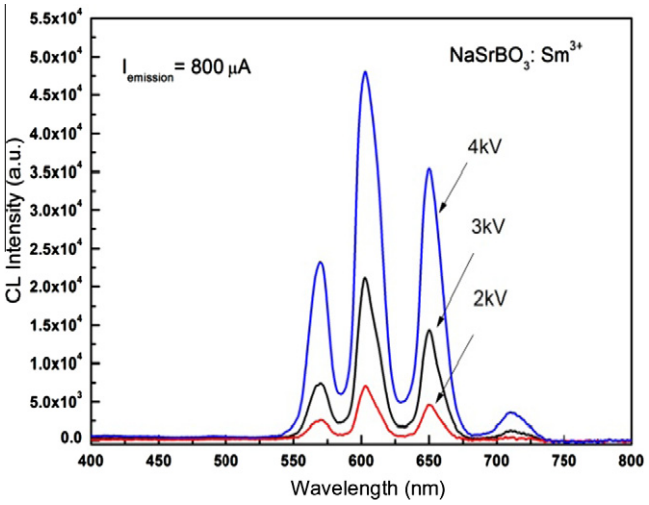

Fig. 5. Cathodoluminescence emission of the $NaSrBO_3$:Sm^{3+} phosphor.

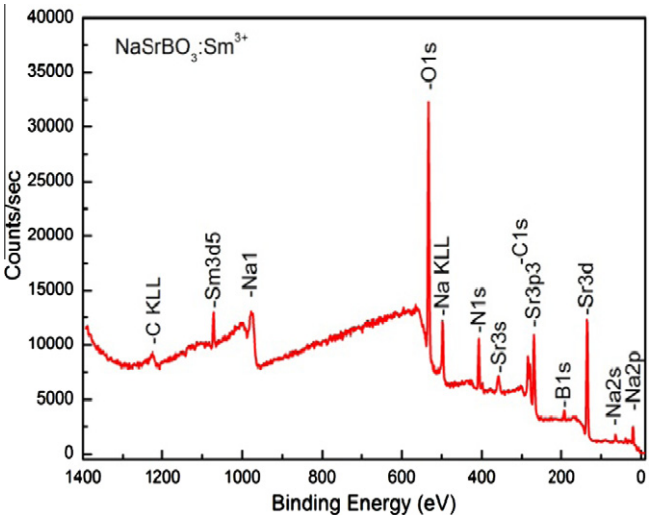

Fig. 8. XPS wide scan for $NaSrBO_3$:Sm^{3+}.

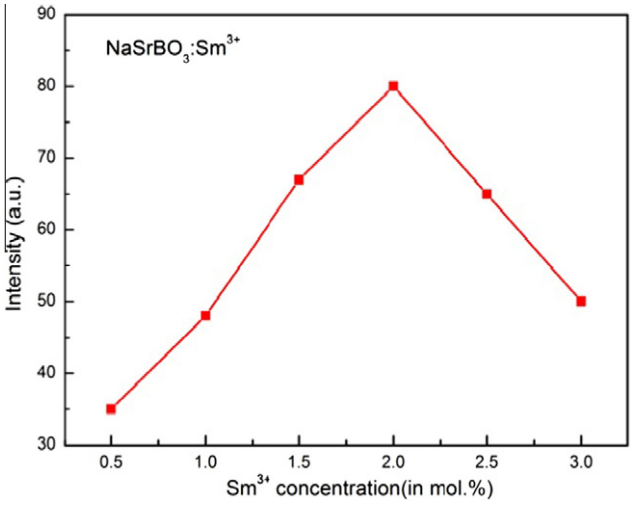

Fig. 6. Variation of the 599 nm PL emission peak as function of Sm^{3+} concentration.

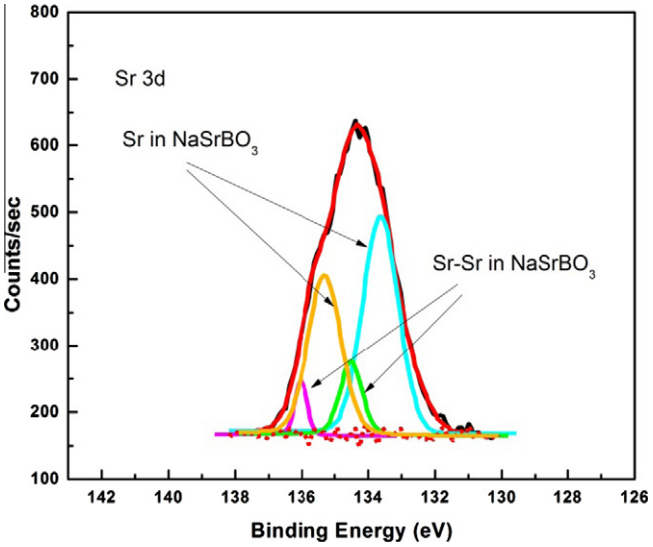

Fig. 9. High resolution XPS scan and deconvolution of the Sr 3d signal.

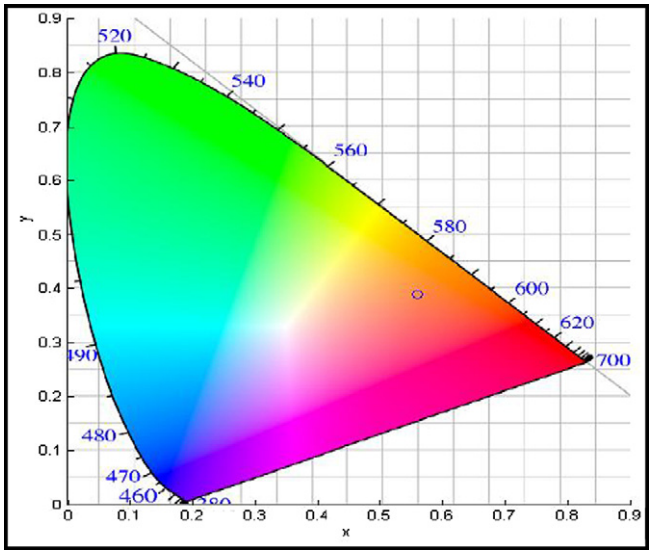

Fig. 7. The CIE 1931 chromaticity diagram for $NaSrBO_3$: Sm^{3+} phosphor under 395 nm excitation.

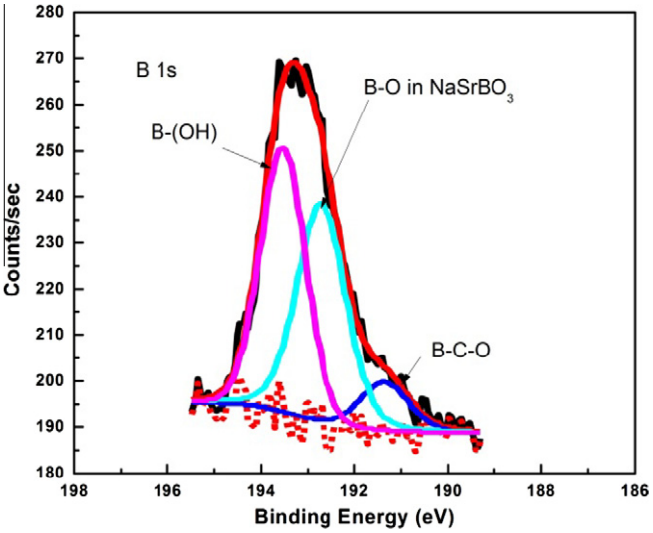

Fig. 10. High resolution XPS scan and deconvolution of the B 1s signal.

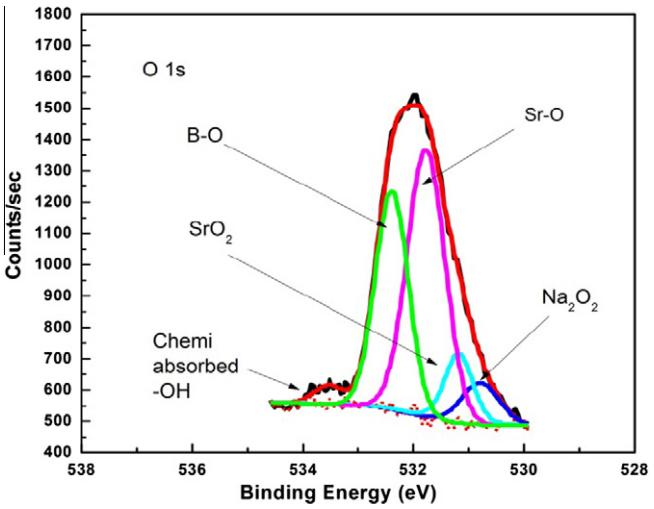

Fig. 11. High resolution XPS scan and deconvolution of the O 1s signal.

3.2. Surface chemical study

X-ray photoelectron spectroscopy (XPS) has proved to be a powerful analytical technique that can be used in material science to study the elemental composition and the oxidation state of the cations. In Fig. 8, the wide scan XPS spectrum of the sample comfirms the presence of Na, Sr, B, O and Sm and their corresponding binding energies.

The XPS high resolution scan with the deconvolution for the Sr 3d core level is shown in Fig. 9. Due to the complete transfer of valence electron from Sr to O atoms, the Sr–O chemical bonds are commonly classified as ionic in nature. Autchin et al. [27] suggested that in Sr bearing oxides, the binding energy (B.E.) of the Sr $3d_{5/2}$ line remains unchanged. Peak fittings of the signal collected from the core scan exhibited two different chemical environments of the Sr. One was attributed to oxygen coordinated Sr in the $NaSrBO_3$ lattice for which the $3d_{5/2}$ and $3d_{3/2}$ spin order split components were located at B.E.'s of 133.2 eV and 135.1 eV. The other component resembles the metallic Sr bonding at B.E.'s of 134.3 eV and 136.1 eV for Sr $3d_{5/2}$ and $3d_{3/2}$, respectively. These peaks can be assigned to Sr residing at interstitial and surface terminated positions of $NaSrBO_3$. Fig. 10 shows the B 1s core level photoelectron spectra in the $NaSrBO_3$ lattice. The lop-sided nature of the peak suggests that a distribution of B chemical states exists. The binding energy of the component at 192.3 eV is attributed to photoelectrons originating from B atoms bonded to oxygen atoms (B–O) in the host lattice. The lower peak at a binding energy (B.E.) around 191.2 eV can be assigned to mixed B–C and B–O bonding (e.g. $B–C_2O$, $B–CO_2$ or $B–CO_3$) [28,29]. The O 1s core level scan in host matrix is deconvoluted into five components representing different lattice sites of oxygen in the $NaSrBO_3$ as shown in Fig. 11. The peak at 530.8 eV, 531.1, 531.7 eV, and 532.2 eV and 533.5 eV correspond to the Na_2O_2, SrO_2, Sr–O, and B–O [30,31] type of bond-

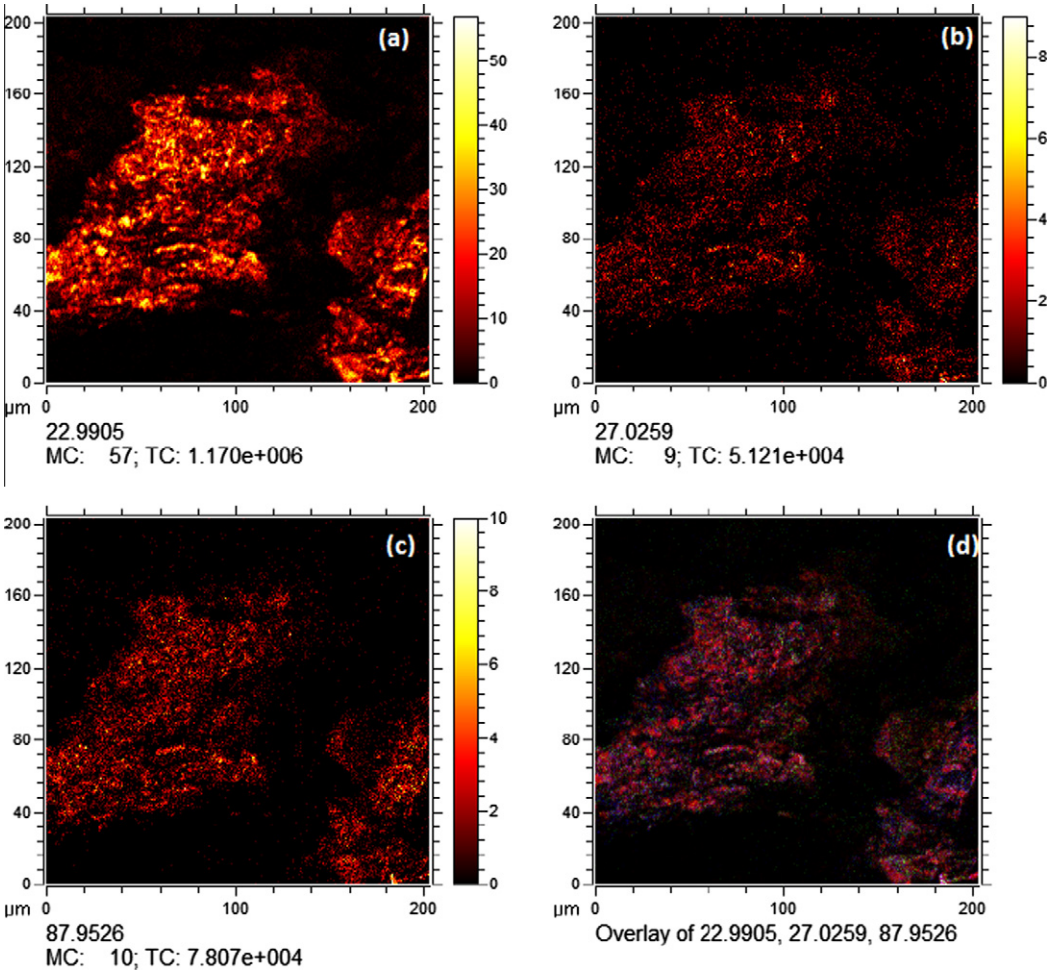

Fig. 12. Chemical color TOF SIMS images of (a) Na^+, (b) BO^+, (c) Sr^+ and (d) the overlay of all.

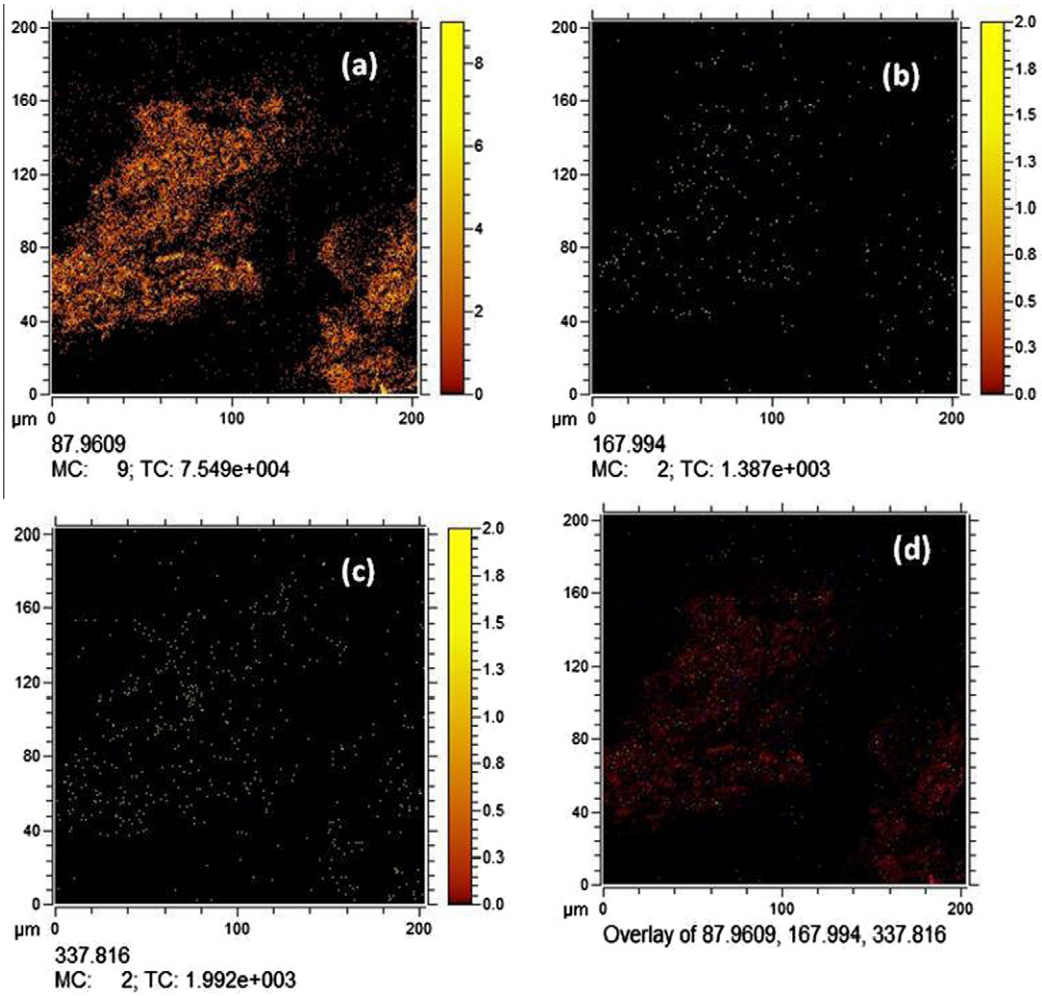

Fig. 13. False color TOF SIMS images of (a) Sr^+, (b) SmO^+ (c) $Sm(NO_3)_3^+$ and (d) overlay of the three.

ing in the sample. The peak at 533.5 eV can be attributed to chemisorbed –OH species on the surface of the $NaSrBO_3$.

The TOF-SIMS offers the possibility of imaging components based on the elemental or isotopic masses of their atomic and molecular ion fragments with high lateral resolution and sensitivity, yielding information including the identification of the peak composition and the distribution of the dopant and the homogeneity of the doping in the host lattice [32,33]. Thus, we used the TOF-SIMS to analyse the composition of the elemental masses. Fig. 12 shows the chemical false color images of an area of 200 µm × 200 µm of the Na^+ 23 u, BO^+ 27 u, Sr^+ 87.9 u, respectively and their overlay. To see the dopant distribution, a separate overlay is shown in Fig. 13 for Sr^+ 87.9 u, SmO^+ 167.994 u and $Sr(NO_3)^{3+}$ 337.816 u. It was not possible to measure Sm^+ ions and therefore ions such as the $Sm(NO_3)_3^+$ and SmO^+ were measured. The relative sensitivity of the two ions is different and it is not known which ion is more favorable to be removed from the phosphor structure, therefore a difference in the amounts is expected. It can be seen from the images that the dopant ions (Fig. 13b) are distributed uniformly inside the host matrix (overlay Fig. 13d). This confirms a successful doping with Sm^{3+} ions over the scan area of 200 µm × 200 µm in the $NaSrBO_3$ host. Some hydrocarbon signals are observed across the surface of the phosphor particles which superficially arises from contamination produced during the process of sample mounting and handling. TOF-SIMS was successfully used in the past to obtain the relative distribution of the dopants in a $Sr_5(PO_4)_3F$ host matrix [34].

4. Conclusions

In summary, the combustion method was used to synthesis the $NaSrBO_3$:Sm^{3+} phosphors. Their structural, spectral and surface properties were discussed. The phosphors were excited with 395 nm, which matched well with the emission wavelength of a UV-chip. Its potential to fabricate LEDs using these chips can be explored. With this excitation, the materials showed a strong orange–red (amber) emission due to the $^4G_{5/2} \rightarrow {}^6H_{7/2}$ transition of the Sm^{3+} ion. This is therefore a very suitable phosphor that may be used as a down conversion phosphor to fill the "yellow gap". The high CL intensity emission also suggest a possible application of this phosphor in displays especially FEDs where the prime operating conditions are the low electron beam accelerating voltage and the high current densities. XPS studies also reveal the formation of the host matrix and confirm the incorporation of the Sm^{3+} in the host. This was also verified with surface sensitive ToF-SIMS chemical imaging data. The images suggested a uniform distribution of the Sm^{3+} ions in the $NaSrBO_3$.

Acknowledgements

We are very thankful to South African National Research Foundation (NRF) for providing the *National nano surface characterization facilities* at the University of the Free State, South Africa. One of the authors, AKB is highly thankful to Inter University Accelera-

tor Centre, New Delhi for financial support in the form of fellowship under UFR project code – MS/30505. V K gratefully thanks Department of Science and Technology (DST), Govt. of India for funding the Fast Track Project reference No. SR/FTP/PS-043/2011 under DST Young Scientist Scheme.

References

[1] Z.L. Wang, Y.L. Zhang, L. Xiong, X.F. Li, J.M. Guo, M.L. Gong, Curr. Appl. Phys. 12 (2012) 1084–1087.
[2] C. Guo, J. Yu, X. Ding, M. Li, Z. Ren, J. Bai, J. Electrochem. Soc. 158 (2011) J42–J49.
[3] W.R. Liu, C.H. Huang, C.P. Wu, Y.C. Chiu, Y.T. Yeh, T.M. Chen, J. Mater. Chem. 21 (2011) 6869–6874.
[4] F.Q. Ren, D.H. Chen, Opt. Laser Tech. 42 (2010) 110–114.
[5] S.S. Pitale, I.M. Nagpure, Vinay Kumar, O.M. Ntwaeaborwa, J.J. Terblans, H.C. Swart, Mater. Res. Bull. 46 (2011) 987–994.
[6] S.R. Anishia, M.T. Jose, O. Annalakshmi, V. Ponnusamy, V. Ramasamy, J. Lumin. 130 (2010) 1834–1840.
[7] L.H. Jiang, Y.L. Zhang, C.Y. Li, R. Pang, J.Q. Hao, Q. Su, J. Lumin. 128 (2008) 1904–1908.
[8] S. Das, A.A. Reddy, S.S. Babu, G.V. Prakash, J. Mater. Sci. 46 (2011) 7770–7775.
[9] S. Das, A.A. Reddy, G.V. Prakash, Chem. Phys. Lett. 504 (2011) 206–210.
[10] P. Li, Z. Wang, Z. Yang, Q. Guo, G. Fu, Mater. Res. Bull. 44 (2009) 2068–2071.
[11] K.K. Shaat, H.C. Swart, O.M. Ntwaeaborwa, Opt. Mater. Express 2 (7) (2012) 962–968.
[12] C. Liu, Y. Wang, Y. Hu, R. Chen, F. Liao, J. Alloys Comp. 470 (1–2) (2009) 473–476.
[13] L. Wu, X.L. Chen, Y. Zhang, Y.F. Kong, J.J. Xu, Y.P. Xu, J. Solid State Chem. 179 (2006) 1219–1224.
[14] Y. Wu, D. Ding, S. Pan, F. Yang, G. Ren, J. Alloys Comp. 509 (2011) 7186–7191.
[15] Regina Mueller-Mach, Gerd O. Mueller, Michael R. Krames, Oleg B. Shchekin, Peter J. Schmidt, Helmut Bechtel, Ching-Hui Chen, Oliver Steigelmann, Phys. Status Solidi RRL 3 (7–8) (2009) 215–217.
[16] Michael R. Krames, Oleg B. Shchekin, Regina Mueller-Mach, Gerd O. Mueller, Ling Zhou, Gerard Harbers, M. George Craford, J. Disp. Technol. 3 (2) (2007) 160–175.
[17] Regina Mueller-Mach, Gerd O. Mueller, Troy A. Trottier, Michael R. Krames, A. Kim, Dan A. Steigerwald, SPIE 4776 (2002) 131.
[18] R. Mueller-Mach, IEEE J. Sel. Top. Quantum Electron. 8 (2) (2002) 339–345.
[19] (a) S. Nakamura, G. Fasol, The Blue Laser Diode, Springer, Berlin, 1997;
(b) S. Nakamura, MRS Bull. 29 (1997).
[20] D. Tu, Y. Liang, R. Liu, Z. Cheng, F. Yang, W. Yang, J. Alloys Comp. 509 (2011) 5596–5599.
[21] P.A. Nagpure, S.K. Omanwar, J. Rare Earths 30 (2012) 856.
[22] W.D. Cheng, H. Zhang, Q.S. Lin, F.K. Zheng, J.T. Chen, Chem. Mater. 13 (2001) 1841–1847.
[23] B.D. Cullity, Element of X-ray Diffraction, second ed., Addison-Wesley, New York, 1956. p. 99.
[24] H. Liang, Ye. Tao, Q. Su, S. Wang, J. Solid State Chem. 167 (2002) 435–440.
[25] G. Li, Z. Hou, C. Peng, W. Wang, Z. Cheng, C. Li, H. Lian, J. Lin, Adv. Funct. Mater. 20 (2010) 3446–3456.
[26] G. Blasse, B.C. Grabmaier, Luminescent Materials, Springer-Verlag, 1994.
[27] V.V. Autchin, J.C. Grivel, A.S. Korotkov, Z. Zhang, J. Solid State Chem. 181 (2008) 1285–1291.
[28] M.M. Ennaceur, B. Terreault, J. Nucl. Mater. 280 (2000) 33–38.
[29] Y.S. Liu, L.T. Zhang, L.F. Cheng, W.B. Yang, Y.D. Xu, Appl. Surf. Sci. 255 (2009) 8761–8768.
[30] H.V. Doveren, J.A. Verhoeven, J. Electron Spectrosc. Relat. Phenom. 21 (1980) 265–273.
[31] C.H. Hsieh, H. Jain, A.C. Miller, E.I. Kamitsos, J. Non-Cryst. Solids 168 (1994) 247–257.
[32] N. Winograd, B.J. Garrison, in: A.W. Czanderna, D.M. Hercules (Eds.), Methods of Surface Characterization, vol. 2, Plenum, New York, 1991, p. 45.
[33] B.R. Chakraborty, D. Haranath, H. Chander, S. Hellweg, S. Dambach, H.F. Arlinghaus, Nanotechnology 16 (2005) 1006–1015.
[34] H.C. Swart, I.M. Nagpure, O.M. Ntwaeaborwa, G.L. Fisher, J.J. Terblans, Opt. Express 20 (15) (2012) 17119–17125.